

Measurement of the cross section and longitudinal double-spin asymmetry for di-jet production in polarized pp collisions at $\sqrt{s} = 200$ GeV

L. Adamczyk,¹ J. K. Adkins,¹⁹ G. Agakishiev,¹⁷ M. M. Aggarwal,³¹ Z. Ahammed,⁴⁹ I. Alekseev,^{15, 26} D. M. Anderson,⁴² R. Aoyama,⁴⁶ A. Aparin,¹⁷ D. Arkhipkin,³ E. C. Aschenauer,³ M. U. Ashraf,⁴⁵ A. Attri,³¹ G. S. Averichev,¹⁷ X. Bai,⁷ V. Bairathi,²⁷ R. Bellwied,⁴⁴ A. Bhasin,¹⁶ A. K. Bhati,³¹ P. Bhattarai,⁴³ J. Bielcik,¹⁰ J. Bielcikova,¹¹ L. C. Bland,³ I. G. Bordyuzhin,¹⁵ J. Bouchet,¹⁸ J. D. Brandenburg,³⁶ A. V. Brandin,²⁶ D. Brown,²³ I. Bunzarov,¹⁷ J. Butterworth,³⁶ H. Caines,⁵³ M. Calderón de la Barca Sánchez,⁵ J. M. Campbell,²⁹ D. Cebra,⁵ I. Chakaberia,³ P. Chaloupka,¹⁰ Z. Chang,⁴² A. Chatterjee,⁴⁹ S. Chattopadhyay,⁴⁹ X. Chen,²¹ J. H. Chen,³⁹ J. Cheng,⁴⁵ M. Cherney,⁹ W. Christie,³ G. Contin,²² H. J. Crawford,⁴ S. Das,¹³ L. C. De Silva,⁹ R. R. Debbé,³ T. G. Dedovich,¹⁷ J. Deng,³⁸ A. A. Derevschikov,³³ L. Didenko,³ C. Dilks,³² X. Dong,²² J. L. Drachenberg,²⁰ J. E. Draper,⁵ C. M. Du,²¹ L. E. Dunkelberger,⁶ J. C. Dunlop,³ L. G. Efimov,¹⁷ N. Elsey,⁵¹ J. Engelage,⁴ G. Eppley,³⁶ R. Esha,⁶ S. Esumi,⁴⁶ O. Evdokimov,⁸ J. Ewigleben,²³ O. Eyser,³ R. Fatemi,¹⁹ S. Fazio,³ P. Federic,¹¹ P. Federicova,¹⁰ J. Fedorisin,¹⁷ Z. Feng,⁷ P. Filip,¹⁷ Y. Fisyak,³ C. E. Flores,⁵ L. Fulek,¹ C. A. Gagliardi,⁴² D. Garand,³⁴ F. Geurts,³⁶ A. Gibson,⁴⁸ M. Girard,⁵⁰ L. Greiner,²² D. Grosnick,⁴⁸ D. S. Gunaratne,⁴¹ Y. Guo,¹⁸ S. Gupta,¹⁶ A. Gupta,¹⁶ W. Gurny,³ A. I. Hamad,¹⁸ A. Hamed,⁴² R. Haque,²⁷ J. W. Harris,⁵³ L. He,³⁴ S. Heppelmann,³² S. Heppelmann,⁵ A. Hirsch,³⁴ G. W. Hoffmann,⁴³ S. Horvat,⁵³ X. Huang,⁴⁵ B. Huang,⁸ T. Huang,²⁸ H. Z. Huang,⁶ P. Huck,⁷ T. J. Humanic,²⁹ G. Igo,⁶ W. W. Jacobs,¹⁴ A. Jentsch,⁴³ J. Jia,^{3, 40} K. Jiang,³⁷ S. Jowzaee,⁵¹ E. G. Judd,⁴ S. Kabana,¹⁸ D. Kalinkin,¹⁴ K. Kang,⁴⁵ K. Kauder,⁵¹ H. W. Ke,³ D. Keane,¹⁸ A. Kechechyan,¹⁷ Z. Khan,⁸ D. P. Kikola,⁵⁰ I. Kisel,¹² A. Kisiel,⁵⁰ L. Kochenda,²⁶ D. D. Koetke,⁴⁸ L. K. Kosarzewski,⁵⁰ A. F. Kraishan,⁴¹ P. Kravtsov,²⁶ K. Krueger,² N. Kulathunga,⁴⁴ L. Kumar,³¹ R. Lacey,⁴⁰ M. A. C. Lamont,³ J. M. Landgraf,³ K. D. Landry,⁶ J. Lauret,³ A. Lebedev,³ R. Lednicky,¹⁷ J. H. Lee,³ W. Li,³⁹ C. Li,³⁷ X. Li,³⁷ Y. Li,⁴⁵ X. Li,⁴¹ T. Lin,¹⁴ M. A. Lisa,²⁹ F. Liu,⁷ Y. Liu,⁴² T. Ljubicic,³ W. J. Llope,⁵¹ M. Lomnitz,¹⁸ R. S. Longacre,³ X. Luo,⁷ S. Luo,⁸ Y. G. Ma,³⁹ G. L. Ma,³⁹ R. Ma,³ L. Ma,³⁹ N. Magdy,⁴⁰ R. Majka,⁵³ A. Manion,²² S. Margetis,¹⁸ C. Markert,⁴³ H. S. Matis,²² D. McDonald,⁴⁴ S. McKinzie,²² K. Meehan,⁵ J. C. Mei,³⁸ Z. W. Miller,⁸ N. G. Minaev,³³ S. Mioduszewski,⁴² D. Mishra,²⁷ B. Mohanty,²⁷ M. M. Mondal,⁴² D. A. Morozov,³³ M. K. Mustafa,²² Md. Nasim,⁶ T. K. Nayak,⁴⁹ G. Nigmatkulov,²⁶ T. Niida,⁵¹ L. V. Nogach,³³ T. Nonaka,⁴⁶ J. Novak,²⁵ S. B. Nurushiev,³³ G. Odyniec,²² A. Ogawa,³ K. Oh,³⁵ V. A. Okorokov,²⁶ D. Olivett Jr.,⁴¹ B. S. Page,³ R. Pak,³ Y. X. Pan,⁶ Y. Pandit,⁸ Y. Panebratsev,¹⁷ B. Pawlik,³⁰ H. Pei,⁷ C. Perkins,⁴ P. Pile,³ J. Pluta,⁵⁰ K. Poniatowska,⁵⁰ J. Porter,²² M. Posik,⁴¹ A. M. Poskanzer,²² N. K. Pruthi,³¹ M. Przybycien,¹ J. Putschke,⁵¹ H. Qiu,³⁴ A. Quintero,⁴¹ S. Ramachandran,¹⁹ R. L. Ray,⁴³ R. Reed,^{23, 23} M. J. Rehbein,⁹ H. G. Ritter,²² J. B. Roberts,³⁶ O. V. Rogachevskiy,¹⁷ J. L. Romero,⁵ J. D. Roth,⁹ L. Ruan,³ J. Rusnak,¹¹ O. Rusnakova,¹⁰ N. R. Sahoo,⁴² P. K. Sahu,¹³ I. Sakrejda,²² S. Salur,²² J. Sandweiss,⁵³ J. Schambach,⁴³ R. P. Scharenberg,³⁴ A. M. Schmah,²² W. B. Schmidke,³ N. Schmitz,²⁴ J. Seger,⁹ P. Seyboth,²⁴ N. Shah,³⁹ E. Shabaliev,¹⁷ P. V. Shanmuganathan,²³ M. Shao,³⁷ B. Sharma,³¹ A. Sharma,¹⁶ M. K. Sharma,¹⁶ W. Q. Shen,³⁹ Z. Shi,²² S. S. Shi,⁷ Q. Y. Shou,³⁹ E. P. Sichtermann,²² R. Sikora,¹ M. Simko,¹¹ S. Singha,¹⁸ M. J. Skoby,¹⁴ N. Smirnov,⁵³ D. Smirnov,³ W. Solyst,¹⁴ L. Song,⁴⁴ P. Sorensen,³ H. M. Spinka,² B. Srivastava,³⁴ T. D. S. Stanislaus,⁴⁸ M. Stepanov,³⁴ R. Stock,¹² M. Strikhanov,²⁶ B. Stringfellow,³⁴ T. Sugiura,⁴⁶ M. Sumner,¹¹ B. Summa,³² Z. Sun,²¹ X. M. Sun,⁷ Y. Sun,³⁷ B. Surrow,⁴¹ D. N. Svirida,¹⁵ A. H. Tang,³ Z. Tang,³⁷ A. Taranenko,²⁶ T. Tarnowsky,²⁵ A. Tawfik,⁵² J. Thäder,²² J. H. Thomas,²² A. R. Timmins,⁴⁴ D. Tlustý,³⁶ T. Todoroki,³ M. Tokarev,¹⁷ S. Trentalange,⁶ R. E. Tribble,⁴² P. Tribedy,³ S. K. Tripathy,¹³ O. D. Tsai,⁶ T. Ullrich,³ D. G. Underwood,² I. Upsal,²⁹ G. Van Buren,³ G. van Nieuwenhuizen,³ A. N. Vasiliev,³³ R. Vertesi,¹¹ F. Videbæk,³ S. Vokal,¹⁷ S. A. Voloshin,⁵¹ A. Vossen,¹⁴ G. Wang,⁶ J. S. Wang,²¹ F. Wang,³⁴ Y. Wang,⁴⁵ Y. Wang,⁷ G. Webb,³ J. C. Webb,³ L. Wen,⁶ G. D. Westfall,²⁵ H. Wieman,²² S. W. Wissink,¹⁴ R. Witt,⁴⁷ Y. Wu,¹⁸ Z. G. Xiao,⁴⁵ W. Xie,³⁴ G. Xie,³⁷ K. Xin,³⁶ H. Xu,²¹ Q. H. Xu,³⁸ Y. F. Xu,³⁹ N. Xu,²² Z. Xu,³ J. Xu,⁷ Y. Yang,⁷ S. Yang,³⁷ Y. Yang,²⁸ Y. Yang,²¹ C. Yang,³⁷ Q. Yang,³⁷ Z. Ye,⁸ Z. Ye,⁸ L. Yi,⁵³ K. Yip,³ I. -K. Yoo,³⁵ N. Yu,⁷ H. Zbroszczyk,⁵⁰ W. Zha,³⁷ Y. Zhang,³⁷ J. Zhang,³⁸ X. P. Zhang,⁴⁵ J. B. Zhang,⁷ Z. Zhang,³⁹ S. Zhang,³⁷ J. Zhang,²¹ S. Zhang,³⁹ J. Zhao,³⁴ C. Zhong,³⁹ L. Zhou,³⁷ X. Zhu,⁴⁵ Y. Zoukarnееva,¹⁷ and M. Zyzak¹²

(STAR Collaboration)

¹AGH University of Science and Technology, FPACS, Cracow 30-059, Poland

²Argonne National Laboratory, Argonne, Illinois 60439

³Brookhaven National Laboratory, Upton, New York 11973

- ⁴University of California, Berkeley, California 94720
- ⁵University of California, Davis, California 95616
- ⁶University of California, Los Angeles, California 90095
- ⁷Central China Normal University, Wuhan, Hubei 430079
- ⁸University of Illinois at Chicago, Chicago, Illinois 60607
- ⁹Creighton University, Omaha, Nebraska 68178
- ¹⁰Czech Technical University in Prague, FNSPE, Prague, 115 19, Czech Republic
- ¹¹Nuclear Physics Institute AS CR, 250 68 Prague, Czech Republic
- ¹²Frankfurt Institute for Advanced Studies FIAS, Frankfurt 60438, Germany
- ¹³Institute of Physics, Bhubaneswar 751005, India
- ¹⁴Indiana University, Bloomington, Indiana 47408
- ¹⁵Alikhanov Institute for Theoretical and Experimental Physics, Moscow 117218, Russia
- ¹⁶University of Jammu, Jammu 180001, India
- ¹⁷Joint Institute for Nuclear Research, Dubna, 141 980, Russia
- ¹⁸Kent State University, Kent, Ohio 44242
- ¹⁹University of Kentucky, Lexington, Kentucky, 40506-0055
- ²⁰Lamar University, Physics Department, Beaumont, Texas 77710
- ²¹Institute of Modern Physics, Chinese Academy of Sciences, Lanzhou, Gansu 730000
- ²²Lawrence Berkeley National Laboratory, Berkeley, California 94720
- ²³Lehigh University, Bethlehem, PA, 18015
- ²⁴Max-Planck-Institut für Physik, Munich 80805, Germany
- ²⁵Michigan State University, East Lansing, Michigan 48824
- ²⁶National Research Nuclear University MEPhI, Moscow 115409, Russia
- ²⁷National Institute of Science Education and Research, Bhubaneswar 751005, India
- ²⁸National Cheng Kung University, Tainan 70101
- ²⁹Ohio State University, Columbus, Ohio 43210
- ³⁰Institute of Nuclear Physics PAN, Cracow 31-342, Poland
- ³¹Panjab University, Chandigarh 160014, India
- ³²Pennsylvania State University, University Park, Pennsylvania 16802
- ³³Institute of High Energy Physics, Protvino 142281, Russia
- ³⁴Purdue University, West Lafayette, Indiana 47907
- ³⁵Pusan National University, Pusan 46241, Korea
- ³⁶Rice University, Houston, Texas 77251
- ³⁷University of Science and Technology of China, Hefei, Anhui 230026
- ³⁸Shandong University, Jinan, Shandong 250100
- ³⁹Shanghai Institute of Applied Physics, Chinese Academy of Sciences, Shanghai 201800
- ⁴⁰State University Of New York, Stony Brook, NY 11794
- ⁴¹Temple University, Philadelphia, Pennsylvania 19122
- ⁴²Texas A&M University, College Station, Texas 77843
- ⁴³University of Texas, Austin, Texas 78712
- ⁴⁴University of Houston, Houston, Texas 77204
- ⁴⁵Tsinghua University, Beijing 100084
- ⁴⁶University of Tsukuba, Tsukuba, Ibaraki, Japan,
- ⁴⁷United States Naval Academy, Annapolis, Maryland, 21402
- ⁴⁸Valparaiso University, Valparaiso, Indiana 46383
- ⁴⁹Variable Energy Cyclotron Centre, Kolkata 700064, India
- ⁵⁰Warsaw University of Technology, Warsaw 00-661, Poland
- ⁵¹Wayne State University, Detroit, Michigan 48201
- ⁵²World Laboratory for Cosmology and Particle Physics (WLCAPP), Cairo 11571, Egypt
- ⁵³Yale University, New Haven, Connecticut 06520

(Dated: June 17, 2019)

We report the first measurement of the longitudinal double-spin asymmetry A_{LL} for mid-rapidity di-jet production in polarized pp collisions at a center-of-mass energy of $\sqrt{s} = 200$ GeV. The di-jet cross section was measured and is shown to be consistent with next-to-leading order (NLO) perturbative QCD predictions. A_{LL} results are presented for two distinct topologies, defined by the jet pseudorapidities, and are compared to predictions from several recent NLO global analyses. The measured asymmetries, the first such correlation measurements, support those analyses that find positive gluon polarization at the level of roughly 0.2 over the region of Bjorken- $x > 0.05$.

PACS numbers: 13.87.Ce, 13.88.+e, 14.20.Dh, 14.70.Dj, 13.85.-t

Determining the helicity distribution of the gluons within a proton as a function of momentum fraction,

$\Delta g(x)$, remains an important challenge in high-energy nuclear physics. We do not yet understand the decomposition of the proton's spin into contributions from the spins and orbital angular momenta of its internal quarks and gluons, although high-precision, polarized deep-inelastic scattering (DIS) experiments [1] have shown that less than a third is due to the summed intrinsic spins of the quarks and anti-quarks for $x \gtrsim 10^{-3}$ [2–5]. These fixed-target polarized DIS data only weakly constrain the gluon polarization from inclusive measurements through scaling violations due to the limited coverage of photon virtuality Q^2 .

The Relativistic Heavy Ion Collider (RHIC) has enabled more direct studies of gluons by colliding beams of high-energy polarized protons [6], which directly involve gluons via the quark-gluon (qg) and gluon-gluon (gg) scattering processes that dominate at RHIC pp energies [7]. To date, the tightest constraints on $\Delta g(x)$ and its integral over moderate gluon momentum fractions, $x > 0.05$, are provided by next-to-leading-order (NLO) perturbative QCD (pQCD) global analyses that incorporate the inclusive jet [8–11] and π^0 [12–14] longitudinal double-spin asymmetries measured by STAR and PHENIX, respectively, at RHIC. The most recent such analyses [15, 16] now find compelling evidence for positive gluon polarization of roughly 0.2 over the range $x > 0.05$; they also demonstrate the importance of the RHIC data in reaching this conclusion.

Inclusive jet and π^0 measurements, however, necessarily integrate over a large range in x of the initial state partons for a given transverse momentum, p_T , of the final state. To gain more direct sensitivity to the x dependence of Δg , correlation measurements, such as di-jet production, are required, as these more tightly constrain the kinematics of the colliding partons. At leading order in QCD, the di-jet invariant mass is proportional to the square-root of the product of the initial state momentum fractions, $M = \sqrt{s}\sqrt{x_1 x_2}$, while the sum of the jet pseudorapidities determines their ratio, $\eta_1 + \eta_2 = \ln(x_1/x_2)$.

In this letter, we report the cross section as well as the first measurement of the longitudinal double-spin asymmetry, A_{LL} , for di-jets produced in longitudinally polarized $\vec{p} + \vec{p}$ collisions at $\sqrt{s} = 200$ GeV, based on data recorded in 2009 by the STAR collaboration. The asymmetry result was obtained from a data set of integrated luminosity 21 pb^{-1} ; the cross section is based on a 19 pb^{-1} subset of these data. The polarization of each of the two colliding proton beams, denoted blue (B) and yellow (Y), was determined for each RHIC fill using proton-carbon-based Coulomb-Nuclear Interference polarimeters [17], which were calibrated using a polarized hydrogen gas-jet target [18]. The luminosity-weighted average polarizations of the two beams were $P_B = 56\%$ and $P_Y = 57\%$. The A_{LL} analysis took into account the decay of beam polarization over the course of a RHIC fill. The product $P_B P_Y$ used in the asymmetry measurement

had a relative uncertainty of 6.5% [19].

The STAR detector subsystems used to reconstruct jets are the Time Projection Chamber (TPC) and the Barrel and Endcap Electromagnetic Calorimeters (BEMC, EEMC) [20]. The TPC provides charged particle tracking in a 0.5 T solenoidal magnetic field over the range $|\eta| \lesssim 1.3$ in pseudorapidity and 2π in azimuthal angle ϕ . The BEMC and EEMC are segmented lead-scintillator sampling calorimeters, which provide full azimuthal coverage for $|\eta| < 1$ and $1.09 < \eta < 2$, respectively. The calorimeters measure electromagnetic energy deposition and provide the primary triggering information via fixed $\Delta\eta \times \Delta\phi = 1 \times 1$ calorimeter regions called jet patches. A jet patch trigger was satisfied if the transverse energy in a single jet patch exceeded either 5.4 GeV (JP1 trigger) or 7.3 GeV (JP2 trigger), or if two jet patches adjacent in azimuth each exceeded 3.5 GeV (AJP trigger). In addition, the Beam-Beam Counters (BBCs) [21] were used in the determination of the integrated luminosity and, along with the zero-degree calorimeters (ZDCs) [20], in the determination of helicity-dependent relative luminosities.

The jet reconstruction procedures for these analyses follow those used in the inclusive jet analysis from 2009 [11]. Jets were found using the anti- k_T algorithm [22] as implemented in the FastJet [23] package, using charged-particle track momenta from the TPC and electromagnetic energy from the calorimeters as inputs. The resolution parameter $R = 0.6$ sets the effective size of the jet in η - ϕ space. To be included in the jet analysis, individual tracks were required to have a $p_T \geq 0.2 \text{ GeV}/c$ and individual calorimeter towers needed $E_T \geq 0.2 \text{ GeV}$. To avoid double-counting jet energy contributions from the TPC and calorimeters, towers with tracks pointing to them had the corresponding track energy p_{TC} subtracted from the E_T of the tower, then negative energies were set to zero [11].

Di-jets were selected by choosing the two jets with the highest p_T from a single event that fell in the pseudorapidity range $-0.8 \leq \eta \leq 0.8$. These jets were required to be more than 120° apart in azimuth. Further conditions were placed on the di-jets in order to ensure they reflected the partonic hard scattering and to reduce the contributions from background. This required that at least one jet contained energy from charged tracks, and di-jets containing tracks with p_T above $30 \text{ GeV}/c$, where TPC momentum resolution is poor, were removed from the analysis. To facilitate comparison with theoretical predictions, an asymmetric condition was placed on the transverse momenta of the jets [7], such that one jet in the pair had $p_T \geq 8.0 \text{ GeV}/c$ and the other had $p_T \geq 6.0 \text{ GeV}/c$. Finally, it was required that at least one jet in the pair point to a jet patch that fired the JP2 or AJP (asymmetry and cross section) or JP1 (asymmetry only) trigger.

To correct for detector effects on the measured jet

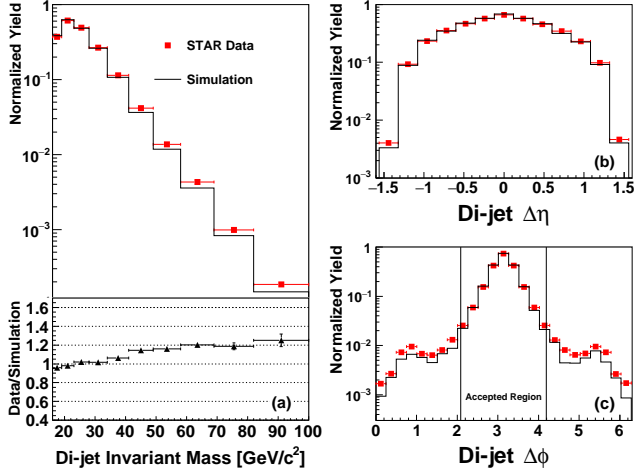


FIG. 1. (Color online) Comparison of di-jet yields as a function of di-jet invariant mass (a), pseudorapidity gap (b), and azimuthal opening angle between the jets (c) in data and Monte Carlo.

quantities and to estimate systematic uncertainties, simulated events were created using PYTHIA 6.425 [24] with the Perugia 0 tune [25] and run through a STAR detector response package implemented in GEANT 3 [26]. The simulated events were embedded into ‘zero-bias’ data events, which were triggered on random bunch crossings over the span of the run, allowing the simulation sample to account properly for the beam background, pile-up, and detector conditions seen in the data set.

Detector-level di-jets were reconstructed from the simulated TPC and calorimeter responses using the same jet-finding algorithm as for the data. Figure 1 compares the distributions of the di-jet invariant mass, as well as the pseudorapidity gap and azimuthal opening angle between the two jets, for di-jets reconstructed from data and simulation, and confirms that the STAR detector response is well understood. Di-jets were also reconstructed in simulation at the particle and parton levels using the anti- k_T algorithm. Particle-level di-jets were formed from stable, final-state particles produced in the simulated event, while parton-level di-jets were reconstructed from the hard-scattered partons emitted in the collision, including initial and final-state radiation, but not beam remnants or underlying event effects as discussed below.

The differential di-jet cross section was calculated at the particle level as a function of invariant mass and pseudorapidity according to

$$\frac{d^3\sigma}{dM d\eta_1 d\eta_2} = \frac{1}{\Delta M \Delta \eta_1 \Delta \eta_2} \frac{J}{\mathcal{L}}, \quad (1)$$

where ΔM and $\Delta \eta$ are the invariant mass and jet pseudorapidity intervals, \mathcal{L} is the integrated luminosity of the sample, and J is the fully corrected di-jet yield. The

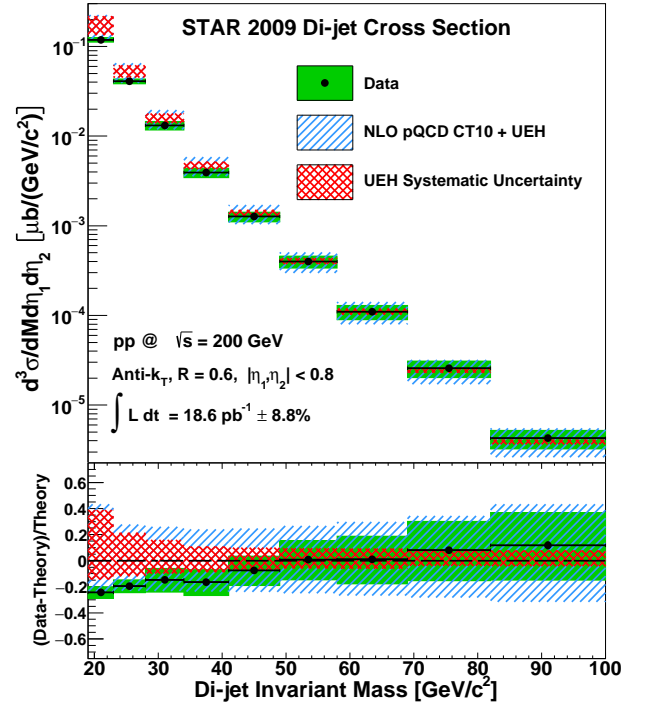


FIG. 2. (Color online) The particle-level di-jet differential cross section measured by the STAR experiment (points plotted at bin center). The lower panel provides a relative comparison to theory, as described in the text.

corrected yield was obtained by unfolding the raw di-jet yield to the particle level using the Singular Value Decomposition (SVD) method as implemented within the RooUnfold package [27], which corrects for bin migration effects due to finite detector resolution and acceptance. The input to SVD is a simulated ‘response matrix’, which relates the mass of di-jets found at the detector level to the mass of the corresponding di-jets at particle level on an event-by-event basis. Di-jet matching between detector and particle level was done by finding the closest particle-level jet in η - ϕ space to each detector-level jet in the event, and requiring these jets to be within $\sqrt{\Delta \eta^2 + \Delta \phi^2} \leq 0.5$. Once the raw yield had been unfolded back to the particle level, a correction for the detector, reconstruction, and trigger efficiencies was applied.

Figure 2 shows the measured di-jet cross section, indicating the associated systematic uncertainty (solid green band) and a theoretical prediction (single-hatched blue band) obtained from the NLO di-jet production code of deFlorian *et al.* [7] using the CT10 parton distribution function (PDF) set [28] (see supplementary material for values [29]). The systematic uncertainty budget of the data contains contributions from uncertainties on track reconstruction efficiency and calorimeter tower energy scale (each ranging from 3% to 15%) as well as uncertainties on track p_T resolution and the unfolding procedure.

In addition to the above (strongly correlated) point-to-point systematics, a systematic of 8.8% common to all points due to uncertainty in the extraction of the integrated luminosity is not included in the height of the systematic uncertainty boxes.

The theoretical cross section was corrected for underlying event and hadronization (UEH) effects. The dominant contribution from the UEH to the di-jet mass is from the individual jet masses [30], which are typically treated as massless in NLO calculations. The UEH correction was estimated from simulation by taking the ratio of the particle-level over parton-level di-jet yields. The ratio ranges from 1.44 at low mass to 1.22 at high mass and is used as a multiplicative correction to the NLO predictions.

The systematic uncertainty on both the UEH correction (double-hatched red band) and the theoretical cross section itself took into account the uncertainty on the PDF set used as well as sensitivity to the variation of the factorization and renormalization scales. The systematic uncertainty on the UEH correction ranged between 39% and 7% from low to high mass, respectively, while the uncertainty on the theory was between 19% and 43%. The height of the blue hatched band represents the quadrature sum of the theoretical and UEH systematics. Note that neither systematic uncertainty is symmetric about its nominal value. Systematic uncertainties on the extracted cross section are smaller than the theoretical uncertainties for all mass bins, meaning these data have the potential to improve our understanding of UEH effects (at low mass) and unpolarized PDFs in our kinematic regime.

Sorting the yields by beam spin state enables a determination of the longitudinal double-spin asymmetry A_{LL} , evaluated as

$$A_{LL} = \frac{\sum (P_Y P_B) (N^{++} - r N^{+-})}{\sum (P_Y P_B)^2 (N^{++} + r N^{+-})}, \quad (2)$$

where $P_{Y,B}$ are the polarizations of the yellow and blue beams, N^{++} and N^{+-} are the di-jet yields from beam bunches with the same and opposite helicity configurations, respectively, and r is the relative integrated luminosity of these configurations. The sum is over individual runs, which ranged from 10 to 60 minutes in length and were short compared to changes in beam conditions. The factor r was close to unity on average, varying between 0.8 and 1.2.

As noted previously, the advantage of a correlation observable over inclusive measurements lies in the former's superior ability to constrain initial state kinematics based on, for example, invariant mass and di-jet topological configurations. The asymmetry A_{LL} is presented for two distinct topologies: 'same-sign' in which both jets have either positive or negative pseudorapidity, and 'opposite-sign' in which one jet has positive and the other

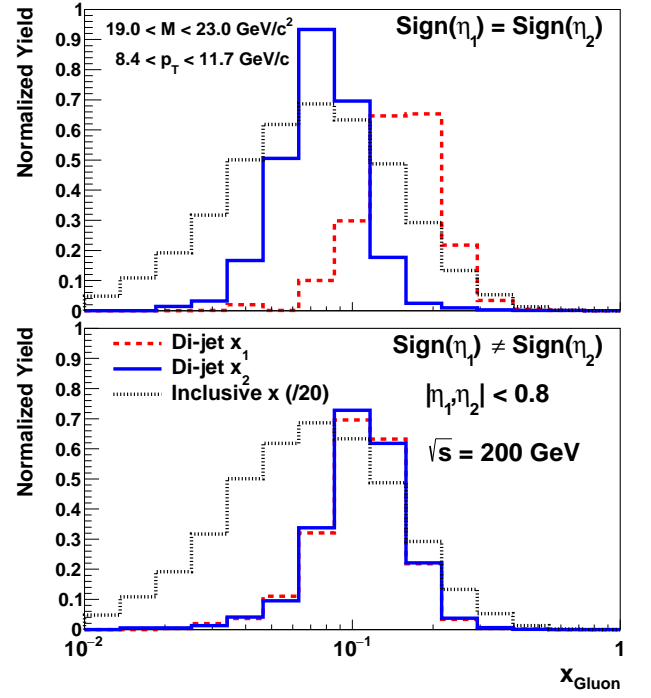


FIG. 3. (Color online) Values of gluon x_1 and x_2 obtained from the PYTHIA detector level simulation for the same-sign (upper) and opposite-sign (lower) di-jet topologies, compared to the gluon x distribution for inclusive jets scaled by an additional factor of 20 in each panel.

negative pseudorapidity. The opposite-sign topology selects events arising from relatively symmetric (in x) partonic collisions, whereas same-sign events select more asymmetric collisions. The most asymmetric, high- p_T collisions are preferentially between a high momentum (high x and therefore highly polarized) quark and a low momentum gluon. The control over initial kinematics achievable with di-jets can be seen in Fig. 3 which presents the partonic momentum fraction distributions (weighted by partonic A_{LL}) of the gluons as obtained from PYTHIA for a sample of detector level di-jets with $19.0 < M < 23.0$ GeV/ c^2 , as well as for inclusive jets with $8.4 < p_T < 11.7$ GeV/ c . The increase in x resolution achievable with di-jets compared to inclusive jets is evident from the much narrower di-jet x distributions. The asymmetric nature of the collisions in the same-sign events (upper plot) can be seen in the separation of the high- and low- x distributions, whereas the opposite-sign events (lower plot) sample an intermediate x range. Other di-jet mass bin choices sample different gluon x regions.

Values of A_{LL} extracted from the data via Eq. 2 represent an admixture of the asymmetries produced from the three dominant partonic scattering sub-processes: qq , qg , and gg . The STAR trigger is more efficient for certain sub-processes [11], altering the sub-process fractions in

the data-set and thereby shifting the measured A_{LL} . Further distortions can arise due to systematic shifts caused by the finite resolution of the detector coupled with a rapidly falling invariant mass distribution. Corrections were applied to the raw A_{LL} values to compensate for these effects. A trigger and reconstruction bias correction was determined by comparing A_{LL} from simulation at the detector and parton levels using several polarized PDFs which predict asymmetries that ‘bracket’ the measured A_{LL} values. Although PYTHIA does not include parton polarization effects, asymmetries were calculated on an event-by-event basis by using the hard scattering kinematics to obtain values from the polarized and unpolarized PDFs. The trigger and reconstruction bias correction in each mass bin was determined by evaluating $\Delta A_{LL} \equiv A_{LL}^{detector} - A_{LL}^{parton}$ for each of the selected PDFs, then taking the average of the minimum and maximum values found. These corrections to A_{LL} varied from 0.0006 at low mass to 0.0048 at high mass. Half of the difference between the minimum and maximum ΔA_{LL} was taken as a systematic uncertainty on the correction.

Figure 4 presents the final di-jet A_{LL} measurement for the same-sign (top) and opposite-sign (bottom) topological configurations as a function of di-jet invariant mass, which has been corrected back to the parton level (see supplementary material for values [29]). The heights of the uncertainty boxes represent the systematic uncertainty on the A_{LL} values due to the trigger and reconstruction bias ($3\text{--}32 \times 10^{-4}$) and residual transverse polarization components in the beams ($3\text{--}26 \times 10^{-4}$). The relative luminosity uncertainty (5×10^{-4}) also results in an uncertainty in the vertical dimension that is common to all points and is represented by the gray band on the horizontal axis. This uncertainty was evaluated by comparing relative luminosity values obtained using the STAR BBCs and ZDCs, as well as from quantitative inspection of a number of single- and double-spin asymmetries expected to yield null results. The widths of the boxes represent the systematic uncertainty associated with the corrected di-jet mass values and, in addition to contributions from the uncertainty on the correction to the parton level, include uncertainties on calorimeter tower gains and efficiencies as well as TPC momentum resolution and tracking efficiencies. A further uncertainty was added in quadrature to account for the difference between the PYTHIA parton level and NLO pQCD di-jet cross sections. This PYTHIA vs. NLO pQCD uncertainty dominates in all but the lowest mass bin, rendering the di-jet mass uncertainties highly correlated.

Theoretical A_{LL} values were obtained from the di-jet production code of deFlorian *et al.* [7] using the DSSV2014 [15] and NNPDFpol1.1 [16] polarized PDF sets as input, normalized by the MRST2008 [31] and NNPDF2.3 [32] unpolarized sets, respectively. Uncertainty bands representing the sensitivity to factorization and renormalization scale (solid) and polarized PDF un-

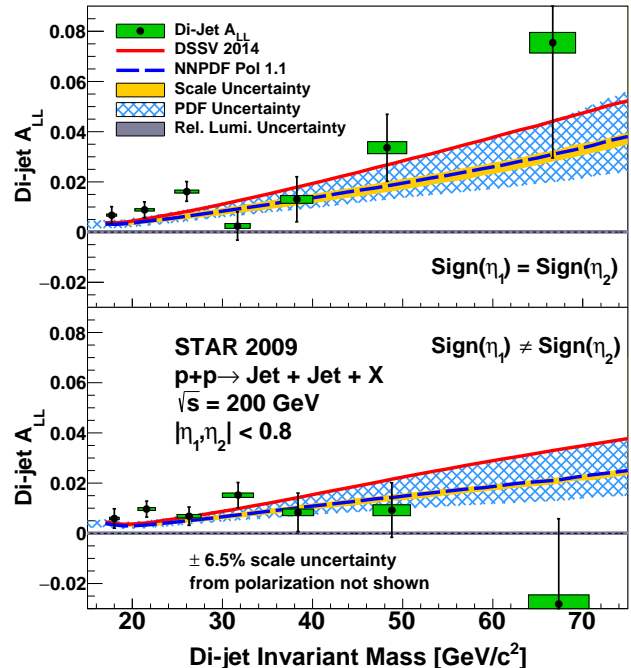


FIG. 4. (Color online) Di-jet A_{LL} for the same-sign (top) and opposite-sign (bottom) topological configurations measured by the STAR experiment. The uncertainty symbols and theoretical curves are explained in the text.

certainty (hatched) were generated for the NNPDF result. Overall, the data show good agreement with both the DSSV (same-sign $\chi^2/\text{NDF} = 9.9/7$, opposite-sign $\chi^2/\text{NDF} = 9.2/7$) and NNPDF (same-sign $\chi^2/\text{NDF} = 12.0/7$, opposite-sign $\chi^2/\text{NDF} = 8.8/7$) predictions. This is to be expected as both global analyses incorporated the STAR 2009 inclusive jet A_{LL} data, of which these results are a subset. However, for both topological configurations, the measured asymmetries tend to lie above the theoretical predictions at low invariant mass. This suggests the di-jet data may prefer a somewhat higher gluon polarization at low x than the current global analyses.

The di-jet asymmetry results presented here represent an important advance in the experimental investigation of the gluon polarization and will be the basis for future high statistics di-jet measurements at STAR. Correlation measurements capture a more complete picture of the hard scattering kinematics and therefore, as shown in Fig. 3, offer better determination of the gluon momentum fraction than is possible with inclusive jet measurements. This improvement in x resolution will allow global analyses to constrain better the behavior of $\Delta g(x)$ as a function of x , thus reducing the uncertainty on extrapolations to poorly measured x regions and, ultimately, the integrated value of $\Delta g(x)$.

In summary, we report the first di-jet unpolarized

cross section and longitudinal double-spin asymmetry measurements from STAR in polarized pp collisions at $\sqrt{s} = 200$ GeV. The cross section result is consistent with NLO pQCD expectations and has the potential to constrain unpolarized PDFs. The A_{LL} results support the most recent DSSV and NNPDF global analyses, which included 2009 RHIC data and found the first non-zero ΔG value for $x > 0.05$, and may indicate a slightly higher gluon polarization at lower x values.

We are grateful to M. Stratmann and R. Sassot for useful discussions. We thank the RHIC Operations Group and RCF at BNL, the NERSC Center at LBNL, the KISTI Center in Korea, and the Open Science Grid consortium for providing resources and support. This work was supported in part by the Office of Nuclear Physics within the U.S. DOE Office of Science, the U.S. NSF, the Ministry of Education and Science of the Russian Federation, NSFC, CAS, MoST and MoE of China, the National Research Foundation of Korea, NCKU (Taiwan), GA and MSMT of the Czech Republic, FIAS of Germany, DAE, DST, and UGC of India, the National Science Centre of Poland, National Research Foundation, the Ministry of Science, Education and Sports of the Republic of Croatia, and RosAtom of Russia.

-
- [1] C. A. Aidala, S. D. Bass, D. Hasch, and G. K. Mallot, Rev. Mod. Phys. **85**, 655 (2013); and references therein.
 - [2] D. de Florian, R. Sassot, M. Stratmann, and W. Vogelsang, Phys. Rev. Lett. **101**, 072001 (2008); Phys. Rev. D **80**, 034030 (2009).
 - [3] J. Blümlein and H. Böttcher, Nucl. Phys. B **841**, 205 (2010).
 - [4] E. Leader, A. V. Sidorov, and D. B. Stamenov, Phys. Rev. D **82**, 114018 (2010).
 - [5] R. D. Ball *et al.* [NNPDF Collaboration], Nucl. Phys. B **874**, 36 (2013).
 - [6] I. Alekseev *et al.*, Nucl. Instrum. Meth. A **499**, 392 (2003).
 - [7] D. de Florian, S. Frixione, A. Signer and W. Vogelsang, Nucl. Phys. B **539**, 455 (1999)
 - [8] B. I. Abelev *et al.* [STAR Collaboration], Phys. Rev. Lett. **97**, 252001 (2006).
 - [9] B. I. Abelev *et al.* [STAR Collaboration], Phys. Rev. Lett. **100**, 232003 (2008).
 - [10] L. Adamczyk *et al.* [STAR Collaboration], Phys. Rev. D **86**, 032006 (2012).
 - [11] L. Adamczyk *et al.* [STAR Collaboration], Phys. Rev. Lett. **115**, 092002 (2015).
 - [12] A. Adare *et al.* [PHENIX Collaboration], Phys. Rev. Lett. **103**, 012003 (2009).
 - [13] A. Adare *et al.* [PHENIX Collaboration], Phys. Rev. D **79**, 012003 (2009).
 - [14] A. Adare *et al.* [PHENIX Collaboration], Phys. Rev. D **90**, 012007 (2014)
 - [15] D. de Florian, R. Sassot, M. Stratmann and W. Vogelsang, Phys. Rev. Lett. **113**, 012001 (2014)
 - [16] E. R. Nocera *et al.* [NNPDF Collaboration], Nucl. Phys. B **887**, 276 (2014)
 - [17] O. Jinnouchi *et al.*, arXiv:nucl-ex/0412053.
 - [18] H. Okada *et al.*, arXiv:hep-ex/0601001.
 - [19] B. Schmidke *et al.*, BNL C-A Dept. Rep. C-A/AP/490, <http://public.bnl.gov/docs/cad/Pages/Home.aspx> (2013).
 - [20] K. H. Ackermann *et al.* [STAR Collaboration], Nucl. Instrum. Meth. A **499**, 624 (2003), and references therein.
 - [21] J. Kirelyuk [for the STAR Collaboration], arXiv:hep-ex/0501072.
 - [22] M. Cacciari, G. P. Salam, and G. Soyez, JHEP **04**, 063 (2008).
 - [23] M. Cacciari, G. P. Salam, and G. Soyez, Eur. Phys. J. C **72**, 1896 (2012).
 - [24] T. Sjostrand, S. Mrenna, and P. Z. Skands, JHEP **05**, 026 (2006).
 - [25] P. Z. Skands, arXiv:0905.3418.
 - [26] GEANT 3.21, CERN Program Library.
 - [27] T. Adye, Proceedings of the PHYSTAT 2011 Workshop, CERN, Geneva, Switzerland, January 2011, CERN-2011-006, pp 313-318
 - [28] H. L. Lai, M. Guzzi, J. Huston, Z. Li, P. M. Nadolsky, J. Pumplin and C.-P. Yuan, Phys. Rev. D **82**, 074024 (2010)
 - [29] See Supplemental Material at [URL will be inserted by publisher] for [tables of values and associated systematic uncertainties].
 - [30] H. Jung, D. Treleani, M. Strikman and N. van Buuren, DESY-PROC-2016-01.
 - [31] A. D. Martin, W. J. Stirling, R. S. Thorne and G. Watt, Eur. Phys. J. C **63**, 189 (2009)
 - [32] R. D. Ball *et al.* [NNPDF Collaboration], Nucl. Phys. B **867**, 244 (2013)